University of Kentucky
UKnowledge

Physics and Astronomy Faculty Publications   Physics and Astronomy

4-28-2017

Measurement of the Cross Section and Longitudinal Double-Spin Asymmetry for Dijet Production in Polarized *pp* Collisions at √s = 200 GeV

L. Adamczyk
AGH University of Science and Technology, Poland

James K. Adkins
University of Kentucky, kevin.adkins@uky.edu

G. Agakishiev
Joint Institute for Nuclear Research, Russia

M. M. Aggarwal
Panjab University, India

Z. Ahammed
Variable Energy Cyclotron Centre, India

See next page for additional authors

Follow this and additional works at: https://uknowledge.uky.edu/physastron_facpub

Part of the Elementary Particles and Fields and String Theory Commons, and the Nuclear Commons

Right click to open a feedback form in a new tab to let us know how this document benefits you.

Repository Citation

Authors

L. Adamczyk, James K. Adkins, G. Agakishiev, M. M. Aggarwal, Z. Ahammed, N. N. Ajitanand, I. Alekseev, D. M. Anderson, R. Aoyama, A. Aparin, D. Arkhipkin, E. C. Aschenauer, M. U. Ashraf, A. Attri, G. S. Averichev, X. Bai, V. Bairathi, K. Barish, A. Behera, R. Bellwied, A. Bhasin, A. K. Bhati, P. Bhattarai, J. Bielcik, J. Bielcikova, L. C. Bland, I. G. Bordyuzhin, J. Bouchet, J. D. Brandenburg, A. V. Brandin, Renee H. Fatemi, and Suvarna Ramachandran

Measurement of the Cross Section and Longitudinal Double-Spin Asymmetry for Dijet Production in Polarized *pp* Collisions at √*s* = 200 GeV

Due to the large number of authors, only the first 30 and the authors affiliated with the University of Kentucky are listed in the author section above. For the complete list of authors, please download this article or visit: https://doi.org/10.1103/PhysRevD.95.071103

This group of authors is collectively known as the STAR Collaboration.

Measurement of the cross section and longitudinal double-spin asymmetry for dijet production in polarized pp collisions at $\sqrt{s} = 200$ GeV

L. Adamczyk,[1] J. K. Adkins,[19] G. Agakishiev,[17] M. M. Aggarwal,[31] Z. Ahammed,[51] N. N. Ajitanand,[40] I. Alekseev,[15,26] D. M. Anderson,[42] R. Aoyama,[46] A. Aparin,[17] D. Arkhipkin,[3] E. C. Aschenauer,[3] M. U. Ashraf,[45] A. Attri,[31] G. S. Averichev,[17] X. Bai,[7] V. Bairathi,[27] K. Barish,[48] A. Behera,[40] R. Bellwied,[44] A. Bhasin,[16] A. K. Bhati,[31] P. Bhattarai,[43] J. Bielcik,[10] J. Bielcikova,[11] L. C. Bland,[3] I. G. Bordyuzhin,[15] J. Bouchet,[18] J. D. Brandenburg,[36] A. V. Brandin,[26] D. Brown,[23] I. Bunzarov,[17] J. Butterworth,[36] H. Caines,[55] M. Calderón de la Barca Sánchez,[5] J. M. Campbell,[29] D. Cebra,[5] I. Chakaberia,[3] P. Chaloupka,[10] Z. Chang,[42] N. Chankova-Bunzarova,[17] A. Chatterjee,[51] S. Chattopadhyay,[51] X. Chen,[37] X. Chen,[21] J. H. Chen,[39] J. Cheng,[45] M. Cherney,[9] W. Christie,[3] G. Contin,[22] H. J. Crawford,[4] S. Das,[7] L. C. De Silva,[9] R. R. Debbe,[3] T. G. Dedovich,[17] J. Deng,[38] A. A. Derevschikov,[33] L. Didenko,[3] C. Dilks,[32] X. Dong,[22] J. L. Drachenberg,[20] J. E. Draper,[5] L. E. Dunkelberger,[6] J. C. Dunlop,[3] L. G. Efimov,[17] N. Elsey,[53] J. Engelage,[4] G. Eppley,[36] R. Esha,[6] S. Esumi,[46] O. Evdokimov,[8] J. Ewigleben,[23] O. Eyser,[3] R. Fatemi,[19] S. Fazio,[3] P. Federic,[11] P. Federicova,[10] J. Fedorisin,[17] Z. Feng,[7] P. Filip,[17] E. Finch,[47] Y. Fisyak,[3] C. E. Flores,[5] J. Fujita,[9] L. Fulek,[1] C. A. Gagliardi,[42] D. Garand,[34] F. Geurts,[36] A. Gibson,[50] M. Girard,[52] D. Grosnick,[50] D. S. Gunarathne,[41] Y. Guo,[18] S. Gupta,[16] A. Gupta,[16] W. Guryn,[3] A. I. Hamad,[18] A. Hamed,[42] A. Harlenderova,[10] J. W. Harris,[55] L. He,[34] S. Heppelmann,[5] S. Heppelmann,[32] A. Hirsch,[34] G. W. Hoffmann,[43] S. Horvat,[55] T. Huang,[28] B. Huang,[8] H. Z. Huang,[6] X. Huang,[45] T. J. Humanic,[29] P. Huo,[40] G. Igo,[6] W. W. Jacobs,[14] A. Jentsch,[43] J. Jia,[3,40] K. Jiang,[37] S. Jowzaee,[53] E. G. Judd,[4] S. Kabana,[18] D. Kalinkin,[14] K. Kang,[45] D. Kapukchyan,[48] K. Kauder,[53] H. W. Ke,[3] D. Keane,[18] A. Kechechyan,[17] Z. Khan,[8] D. P. Kikoła,[52] C. Kim,[48] I. Kisel,[12] A. Kisiel,[52] L. Kochenda,[26] M. Kocmanek,[11] T. Kollegger,[12] L. K. Kosarzewski,[52] A. F. Kraishan,[41] L. Krauth,[48] P. Kravtsov,[26] K. Krueger,[2] N. Kulathunga,[44] L. Kumar,[31] J. Kvapil,[10] J. H. Kwasizur,[14] R. Lacey,[40] J. M. Landgraf,[3] K. D. Landry,[6] J. Lauret,[3] A. Lebedev,[3] R. Lednicky,[17] J. H. Lee,[3] W. Li,[39] C. Li,[37] Y. Li,[45] X. Li,[37] J. Lidrych,[10] T. Lin,[14] M. A. Lisa,[29] H. Liu,[14] F. Liu,[7] Y. Liu,[42] P. Liu,[40] T. Ljubicic,[3] W. J. Llope,[53] M. Lomnitz,[22] R. S. Longacre,[3] X. Luo,[7] S. Luo,[8] R. Ma,[3] G. L. Ma,[39] L. Ma,[39] Y. G. Ma,[39] N. Magdy,[40] R. Majka,[55] D. Mallick,[27] S. Margetis,[18] C. Markert,[43] H. S. Matis,[22] K. Meehan,[5] J. C. Mei,[38] Z. W. Miller,[8] N. G. Minaev,[33] S. Mioduszewski,[42] D. Mishra,[27] S. Mizuno,[22] B. Mohanty,[27] M. M. Mondal,[13] D. A. Morozov,[33] M. K. Mustafa,[22] Md. Nasim,[6] T. K. Nayak,[51] J. M. Nelson,[4] M. Nie,[39] G. Nigmatkulov,[26] T. Niida,[53] L. V. Nogach,[33] T. Nonaka,[46] S. B. Nurushev,[33] G. Odyniec,[22] A. Ogawa,[3] K. Oh,[35] V. A. Okorokov,[26] D. Olvitt, Jr.,[41] B. S. Page,[3] R. Pak,[3] Y. Pandit,[8] Y. Panebratsev,[17] B. Pawlik,[30] H. Pei,[7] C. Perkins,[4] P. Pile,[3] J. Pluta,[52] K. Poniatowska,[52] J. Porter,[22] M. Posik,[41] N. K. Pruthi,[31] M. Przybycien,[1] J. Putschke,[53] H. Qiu,[34] A. Quintero,[41] S. Ramachandran,[19] R. L. Ray,[43] R. Reed,[23] M. J. Rehbein,[9] H. G. Ritter,[22] J. B. Roberts,[36] O. V. Rogachevskiy,[17] J. L. Romero,[5] J. D. Roth,[9] L. Ruan,[3] J. Rusnak,[11] O. Rusnakova,[10] N. R. Sahoo,[42] P. K. Sahu,[13] S. Salur,[22] J. Sandweiss,[55] M. Saur,[11] J. Schambach,[43] A. M. Schmah,[22] W. B. Schmidke,[3] N. Schmitz,[24] B. R. Schweid,[40] J. Seger,[9] M. Sergeeva,[6] R. Seto,[48] P. Seyboth,[24] N. Shah,[39] E. Shahaliev,[17] P. V. Shanmuganathan,[23] M. Shao,[37] A. Sharma,[16] M. K. Sharma,[16] W. Q. Shen,[39] S. S. Shi,[7] Z. Shi,[22] Q. Y. Shou,[39] E. P. Sichtermann,[22] R. Sikora,[1] M. Simko,[11] S. Singha,[18] M. J. Skoby,[14] N. Smirnov,[55] D. Smirnov,[3] W. Solyst,[14] L. Song,[44] P. Sorensen,[3] H. M. Spinka,[2] B. Srivastava,[34] T. D. S. Stanislaus,[50] M. Strikhanov,[26] B. Stringfellow,[34] T. Sugiura,[46] M. Sumbera,[11] B. Summa,[32] X. Sun,[7] X. M. Sun,[7] Y. Sun,[37] B. Surrow,[41] D. N. Svirida,[15] A. H. Tang,[3] Z. Tang,[37] A. Taranenko,[26] T. Tarnowsky,[25] A. Tawfik,[54] J. Thäder,[22] J. H. Thomas,[22] A. R. Timmins,[44] D. Tlusty,[36] T. Todoroki,[3] M. Tokarev,[17] S. Trentalange,[6] R. E. Tribble,[42] P. Tribedy,[3] S. K. Tripathy,[13] B. A. Trzeciak,[10] O. D. Tsai,[6] T. Ullrich,[3] D. G. Underwood,[2] I. Upsal,[29] G. Van Buren,[3] G. van Nieuwenhuizen,[3] A. N. Vasiliev,[33] F. Videbæk,[3] S. Vokal,[17] S. A. Voloshin,[53] A. Vossen,[14] G. Wang,[6] Y. Wang,[45] F. Wang,[34] Y. Wang,[7] G. Webb,[3] J. C. Webb,[3] L. Wen,[6] G. D. Westfall,[25] H. Wieman,[22] S. W. Wissink,[14] R. Witt,[49] Y. Wu,[18] Z. G. Xiao,[45] W. Xie,[34] G. Xie,[37] Y. F. Xu,[39] Q. H. Xu,[38] N. Xu,[22] Z. Xu,[3] J. Xu,[7] Y. Yang,[28] S. Yang,[3] C. Yang,[38] Q. Yang,[37] Z. Ye,[8] Z. Ye,[8] L. Yi,[55] K. Yip,[3] I. -K. Yoo,[35] N. Yu,[7] H. Zbroszczyk,[52] W. Zha,[37] S. Zhang,[39] J. B. Zhang,[7] Y. Zhang,[37] J. Zhang,[21] J. Zhang,[22] S. Zhang,[37] X. P. Zhang,[45] Z. Zhang,[39] J. Zhao,[34] C. Zhong,[39] C. Zhou,[39] L. Zhou,[37] Z. Zhu,[38] X. Zhu,[45] and M. Zyzak[12]

(STAR Collaboration)

[1]*AGH University of Science and Technology, FPACS, Cracow 30-059, Poland*
[2]*Argonne National Laboratory, Argonne, Illinois 60439, USA*
[3]*Brookhaven National Laboratory, Upton, New York 11973, USA*
[4]*University of California, Berkeley, California 94720, USA*
[5]*University of California, Davis, California 95616, USA*
[6]*University of California, Los Angeles, California 90095, USA*
[7]*Central China Normal University, Wuhan, Hubei 430079, China*
[8]*University of Illinois at Chicago, Chicago, Illinois 60607, USA*

[9]Creighton University, Omaha, Nebraska 68178, USA

[10]Czech Technical University in Prague, FNSPE, Prague 115 19, Czech Republic

[11]Nuclear Physics Institute AS CR, 250 68 Prague, Czech Republic

[12]Frankfurt Institute for Advanced Studies FIAS, Frankfurt 60438, Germany

[13]Institute of Physics, Bhubaneswar 751005, India

[14]Indiana University, Bloomington, Indiana 47408, USA

[15]Alikhanov Institute for Theoretical and Experimental Physics, Moscow 117218, Russia

[16]University of Jammu, Jammu 180001, India

[17]Joint Institute for Nuclear Research, Dubna, 141 980, Russia

[18]Kent State University, Kent, Ohio 44242, USA

[19]University of Kentucky, Lexington, Kentucky 40506-0055, USA

[20]Lamar University, Physics Department, Beaumont, Texas 77710, USA

[21]Institute of Modern Physics, Chinese Academy of Sciences, Lanzhou, Gansu 730000, China

[22]Lawrence Berkeley National Laboratory, Berkeley, California 94720, USA

[23]Lehigh University, Bethlehem, Pennsylvania 18015, USA

[24]Max-Planck-Institut fur Physik, Munich 80805, Germany

[25]Michigan State University, East Lansing, Michigan 48824, USA

[26]National Research Nuclear University MEPhI, Moscow 115409, Russia

[27]National Institute of Science Education and Research, Bhubaneswar 751005, India

[28]National Cheng Kung University, Tainan 70101, Taiwan

[29]Ohio State University, Columbus, Ohio 43210, USA

[30]Institute of Nuclear Physics PAN, Cracow 31-342, Poland

[31]Panjab University, Chandigarh 160014, India

[32]Pennsylvania State University, University Park, Pennsylvania 16802, USA

[33]Institute of High Energy Physics, Protvino 142281, Russia

[34]Purdue University, West Lafayette, Indiana 47907, USA

[35]Pusan National University, Pusan 46241, Korea

[36]Rice University, Houston, Texas 77251, USA

[37]University of Science and Technology of China, Hefei, Anhui 230026, China

[38]Shandong University, Jinan, Shandong 250100, China

[39]Shanghai Institute of Applied Physics, Chinese Academy of Sciences, Shanghai 201800, China

[40]State University Of New York, Stony Brook, New York 11794, USA

[41]Temple University, Philadelphia, Pennsylvania 19122, USA

[42]Texas A&M University, College Station, Texas 77843, USA

[43]University of Texas, Austin, Texas 78712, USA

[44]University of Houston, Houston, Texas 77204, USA

[45]Tsinghua University, Beijing 100084, China

[46]University of Tsukuba, Tsukuba, Ibaraki 305-8571, Japan

[47]Southern Connecticut State University, New Haven, Connecticut 06515, USA

[48]University of California, Riverside, California 92521, USA

[49]United States Naval Academy, Annapolis, Maryland 21402, USA

[50]Valparaiso University, Valparaiso, Indiana 46383, USA

[51]Variable Energy Cyclotron Centre, Kolkata 700064, India

[52]Warsaw University of Technology, Warsaw 00-661, Poland

[53]Wayne State University, Detroit, Michigan 48201, USA

[54]World Laboratory for Cosmology and Particle Physics (WLCAPP), Cairo 11571, Egypt

[55]Yale University, New Haven, Connecticut 06520, USA

We report the first measurement of the longitudinal double-spin asymmetry A_{LL} for midrapidity dijet production in polarized pp collisions at a center-of-mass energy of $\sqrt{s} = 200$ GeV. The dijet cross section was measured and is shown to be consistent with next-to-leading order (NLO) perturbative QCD predictions. A_{LL} results are presented for two distinct topologies, defined by the jet pseudorapidities, and are compared to predictions from several recent NLO global analyses. The measured asymmetries, the first such correlation measurements, support those analyses that find positive gluon polarization at the level of roughly 0.2 over the region of Bjorken-$x > 0.05$.

Determining the helicity distribution of the gluons within a proton as a function of momentum fraction, $\Delta g(x)$, remains an important challenge in high-energy nuclear physics. We do not yet understand the decomposition of the proton's spin into contributions from the spins and orbital angular momenta of its internal quarks and gluons, although high-precision, polarized deep-inelastic scattering (DIS) experiments [1] have shown that less than a third is due to the summed intrinsic spins of the quarks and antiquarks for $x \gtrsim 10^{-3}$ [2–5]. These fixed-target polarized DIS data only weakly constrain the gluon polarization from inclusive measurements through scaling violations due to the limited coverage of photon virtuality Q^2.

The Relativistic Heavy Ion Collider (RHIC) has enabled more direct studies of gluons by colliding beams of high-energy polarized protons [6], which directly involve gluons via the quark-gluon (qg) and gluon-gluon (gg) scattering processes that dominate at RHIC pp energies [7]. While leading-order analyses of DIS data with high-p_T hadron pairs have shown hints of positive gluon polarization [8,9], the tightest constraints on $\Delta g(x)$ and its integral over moderate gluon momentum fractions, $x > 0.05$, are provided by next-to-leading-order (NLO) perturbative QCD (pQCD) global analyses that incorporate the inclusive jet [10–13] and π^0 [14–16] longitudinal double-spin asymmetries measured by STAR and PHENIX, respectively, at RHIC. The most recent such analyses [17,18] now find compelling evidence for positive gluon polarization of roughly 0.2 over the range $x > 0.05$; they also demonstrate the importance of the RHIC data in reaching this conclusion.

Inclusive jet and π^0 measurements, however, necessarily integrate over a large range in x of the initial state partons for a given transverse momentum, p_T, of the final state. To gain more direct sensitivity to the x dependence of Δg, correlation measurements, such as dijet production, are required, as these more tightly constrain the kinematics of the colliding partons. At leading order in QCD, the dijet invariant mass is proportional to the square root of the product of the initial state momentum fractions, $M = \sqrt{s}\sqrt{x_1 x_2}$, while the sum of the jet pseudorapidities determines their ratio, $\eta_1 + \eta_2 = \ln(x_1/x_2)$.

In this article, we report the cross section as well as the first measurement of the longitudinal double-spin asymmetry, A_{LL}, for dijets produced in longitudinally polarized $\vec{p} + \vec{p}$ collisions at $\sqrt{s} = 200$ GeV, based on data recorded in 2009 by the STAR Collaboration. The asymmetry result was obtained from a data set of integrated luminosity 21 pb^{-1}; the cross section is based on a 19 pb^{-1} subset of these data. The polarization of each of the two colliding proton beams, denoted blue (B) and yellow (Y), was determined for each RHIC fill using proton-carbon-based Coulomb-nuclear interference polarimeters [19], which were calibrated using a polarized hydrogen gas-jet target [20]. The luminosity-weighted average polarizations of the two beams were $P_B = 56\%$ and $P_Y = 57\%$. The A_{LL}

analysis took into account the decay of beam polarization over the course of a RHIC fill. The product $P_B P_Y$ used in the asymmetry measurement had a relative uncertainty of 6.5% [21].

The STAR detector subsystems used to reconstruct jets are the time projection chamber (TPC) and the barrel and endcap electromagnetic calorimeters (BEMC, EEMC) [22]. The TPC provides charged-particle tracking in a 0.5 T solenoidal magnetic field over the range $|\eta| \lesssim 1.3$ in pseudorapidity and 2π in azimuthal angle ϕ. The BEMC and EEMC are segmented lead-scintillator sampling calorimeters, which provide full azimuthal coverage for $|\eta| < 1$ and $1.09 < \eta < 2$, respectively. The calorimeters measure electromagnetic energy deposition and provide the primary triggering information via fixed $\Delta\eta \times \Delta\phi = 1 \times 1$ calorimeter regions called jet patches. A jet patch trigger was satisfied if the transverse energy in a single jet patch exceeded either 5.4 GeV (JP1 trigger) or 7.3 GeV (JP2 trigger), or if two jet patches adjacent in azimuth each exceeded 3.5 GeV (AJP trigger). Details of the track momentum, and calorimeter energy resolutions can be found in [12]. In addition, the beam-beam counters (BBCs) [23] were used in the determination of the integrated luminosity and, along with the zero-degree calorimeters (ZDCs) [22], in the determination of helicity-dependent relative luminosities.

The jet reconstruction procedures for these analyses follow those used in the inclusive jet analysis from 2009 [13]. Jets were found using the anti-k_T algorithm [24] as implemented in the FastJet [25] package, using charged-particle track momenta from the TPC and electromagnetic energy from the calorimeters as inputs. The resolution parameter $R = 0.6$ sets the effective size of the jet in η-ϕ space. To be included in the jet analysis, individual tracks were required to have a $p_T \geq 0.2$ GeV/c and individual calorimeter towers needed $E_T \geq 0.2$ GeV. To avoid double-counting jet energy contributions from the TPC and calorimeters, towers with tracks pointing to them had the corresponding track energy $p_T c$ subtracted from the E_T of the tower, then negative energies were set to zero. This method results in a jet energy resolution of 18% [13].

Dijets were selected by choosing the two jets with the highest p_T from a single event that fell in the pseudorapidity range $-0.8 \leq \eta \leq 0.8$. These jets were required to be more than 120° apart in azimuth. Further conditions were placed on the dijets in order to ensure they reflected the partonic hard scattering and to reduce the contributions from background. This required that at least one jet contained energy from charged tracks, and dijets containing tracks with p_T above 30 GeV/c, where TPC momentum resolution is poor, were removed from the analysis. The later cut was implemented to eliminate dijets with highly imbalanced jet transverse momenta. These events arose when one track in the event was misreconstructed to have

an artificially high p_T. To facilitate comparison with theoretical predictions, an asymmetric condition was placed on the transverse momenta of the jets [7], such that one jet in the pair had $p_T \geq 8.0$ GeV/c and the other had $p_T \geq 6.0$ GeV/c. Finally, it was required that at least one jet in the pair points to a jet patch that fired the JP2 or AJP (asymmetry and cross section) or JP1 (asymmetry only) trigger.

To correct for detector effects on the measured jet quantities and to estimate systematic uncertainties, simulated events were created using PYTHIA 6.425 [26] with the Perugia 0 tune [27] and run through a STAR detector response package implemented in GEANT 3 [28]. The simulated events were embedded into "zero-bias" data events, which were triggered on random bunch crossings over the span of the run, allowing the simulation sample to account properly for the beam background, pileup, and detector conditions seen in the data set.

Detector-level dijets were reconstructed from the simulated TPC and calorimeter responses using the same jet-finding algorithm as for the data. Figure 1 compares the distributions of the dijet invariant mass, as well as the pseudorapidity gap and azimuthal opening angle between the two jets, for dijets reconstructed from data and simulation, and confirms that the STAR detector response is well understood. Dijets were also reconstructed in simulation at the particle and parton levels using the anti-k_T algorithm. Particle-level dijets were formed from stable, final-state particles produced in the simulated event, while parton-level dijets were reconstructed from the hard-scattered partons emitted in the collision, including initial and final-state radiation, but not beam remnants or underlying event effects as discussed below.

The differential dijet cross section was calculated at the particle level as a function of invariant mass and pseudorapidity according to

$$\frac{d^3\sigma}{dM d\eta_1 d\eta_2} = \frac{1}{\Delta M \Delta\eta_1 \Delta\eta_2} \frac{J}{\mathcal{L}}, \quad (1)$$

where ΔM and $\Delta\eta$ are the invariant mass and jet pseudorapidity intervals, $\mathcal{L}$ is the integrated luminosity of the sample, and J is the fully corrected dijet yield. The corrected yield was obtained by unfolding the raw dijet yield to the particle level using the singular value decomposition (SVD) method as implemented within the RooUnfold package [29], which corrects for bin migration effects due to finite detector resolution and acceptance. The input to SVD is a simulated "response matrix," which relates the mass of dijets found at the detector level to the mass of the corresponding dijets at particle level on an event-by-event basis. Dijet matching between detector and particle level was done by finding the closest particle-level jet in η-ϕ space to each detector-level jet in the event, and requiring these jets to be within $\sqrt{\Delta\eta^2 + \Delta\phi^2} \leq 0.5$. There is a modest but systematic tendency for the detector-level dijet mass to fall below the particle-level mass due to finite track reconstruction efficiency. The mass migration and detector-level purities encoded in the response matrix are given in the Supplemental Material [30]. Once the raw yield had been unfolded back to the particle level, a correction for the detector, reconstruction, and trigger efficiencies was applied.

Figure 2 shows the measured dijet cross section, indicating the associated systematic uncertainty (solid green band) and a theoretical prediction (single-hatched blue bar) obtained from the NLO dijet production code of de Florian *et al.* [7] using the CT10 parton distribution function (PDF) set [31] (see Supplemental Material for values [30]). The theoretical predictions were generated using the same jet algorithm and resolution parameter as the data. The systematic uncertainty budget of the data contains contributions from uncertainties on track reconstruction efficiency and calorimeter tower energy scale (each ranging from 3% to 15%) as well as uncertainties on track p_T resolution and the unfolding procedure. The detector uncertainties were propagated to the cross section by altering the simulated detector response when creating the response matrix, and then using this modified matrix to extract a new cross section. The systematic uncertainty is the difference between the nominal and modified cross sections. In addition to the above (strongly correlated) point-to-point systematics, a systematic of 8.8% common to all points due to uncertainty in the extraction of the integrated luminosity is quoted, but not included in the height of the systematic uncertainty boxes.

The theoretical cross section was corrected for underlying event and hadronization (UEH) effects. The dominant
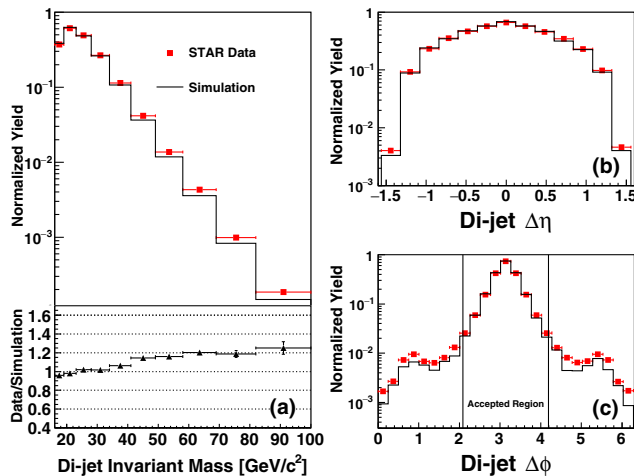

FIG. 1. Comparison of dijet yields as a function of dijet invariant mass (a), pseudorapidity gap (b), and azimuthal opening angle between the jets (c) in data and Monte Carlo. The distributions in (a) and (b) are taken from events within the accepted $\Delta\phi$ region shown in (c).
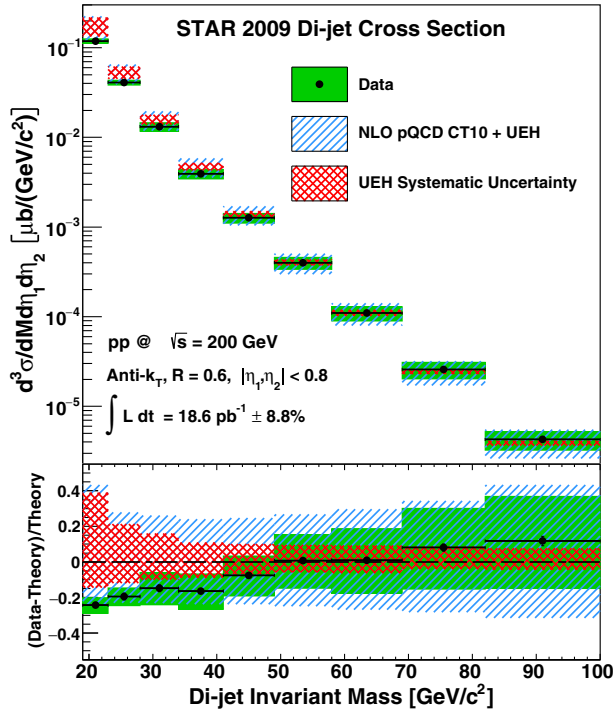
FIG. 2. The particle-level dijet differential cross section measured by the STAR experiment (points plotted at bin center). The lower panel provides a relative comparison to theory, as described in the text.

contribution from the UEH to the dijet mass is from the individual jet masses [32], which are typically treated as massless in NLO calculations. The UEH correction was estimated from simulation by taking the ratio of the particle-level over parton-level dijet yields. The ratio ranges from 1.44 at low mass to 1.22 at high mass and is used as a multiplicative correction to the NLO predictions.

The systematic uncertainty on both the UEH correction (double-hatched red band) and the theoretical cross section itself took into account the uncertainty on the PDF set used as well as sensitivity to the variation of the factorization and renormalization scales, which were altered simultaneously by factors of 0.5 and 2.0. The factorization and renormalization scales were also varied independently between the limits above, but the resulting deviation was always less than the simultaneous case. The systematic uncertainty on the UEH correction ranged between 39% and 7% from low to high mass, respectively, while the uncertainty on the theory was between 19% and 43%. The height of the blue hatched band represents the quadrature sum of the theoretical and UEH systematics. Note that neither systematic uncertainty is symmetric about its nominal value. Systematic uncertainties on the extracted cross section are smaller than the theoretical uncertainties for all mass bins, meaning these data have the potential to improve our understanding of UEH effects (at low mass) and unpolarized PDFs in our kinematic regime.

Sorting the yields by beam spin state enables a determination of the longitudinal double-spin asymmetry A_{LL}, evaluated as

$$A_{LL} = \frac{\sum (P_Y P_B)(N^{++} - rN^{+-})}{\sum (P_Y P_B)^2 (N^{++} + rN^{+-})}, \qquad (2)$$

where $P_{Y,B}$ are the polarizations of the yellow and blue beams, N^{++} and N^{+-} are the dijet yields from beam bunches with the same and opposite helicity configurations, respectively, and r is the relative luminosity of these configurations. The sum is over individual runs, which ranged from 10 to 60 minutes in length and were short compared to changes in beam conditions. The factor r was close to unity on average, varying between 0.8 and 1.2.

As noted previously, the advantage of a correlation observable over inclusive measurements lies in the former's superior ability to constrain initial state kinematics based on, for example, invariant mass and dijet topological configurations. The asymmetry A_{LL} is presented for two distinct topologies: "same-sign" in which both jets have either positive or negative pseudorapidity, and "opposite-sign" in which one jet has positive and the other negative pseudorapidity. The opposite-sign topology selects events arising from relatively symmetric (in x) partonic collisions, whereas same-sign events select more asymmetric collisions. The most asymmetric, high-p_T collisions are preferentially between a high momentum (high x and therefore highly polarized) quark and a low momentum gluon. The control over initial kinematics achievable with dijets can be seen in Fig. 3 which presents the partonic momentum fraction distributions (weighted by partonic A_{LL}) of the gluons as obtained from PYTHIA for a sample of detector level dijets with $19.0 < M < 23.0$ GeV/c^2, as well as for inclusive jets with $8.4 < p_T < 11.7$ GeV/c. The increase in x resolution achievable with dijets compared to inclusive jets is evident from the much narrower dijet x distributions. The asymmetric nature of the collisions in the same-sign events (upper plot) can be seen in the separation of the high- and low-x distributions, whereas the opposite-sign events (lower plot) sample an intermediate x range. Other dijet mass bin choices sample different gluon x regions.

Values of A_{LL} extracted from the data via Eq. (2) represent an admixture of the asymmetries produced from the three dominant partonic scattering subprocesses: qq, qg, and gg. The STAR trigger is more efficient for certain subprocesses [13], altering the subprocess fractions in the data set and thereby shifting the measured A_{LL}. Further distortions can arise due to systematic shifts caused by the finite resolution of the detector coupled with a rapidly falling invariant mass distribution. Corrections were applied to the raw A_{LL} values to compensate for these effects. A trigger and reconstruction bias correction was determined by comparing A_{LL} from simulation at the detector and parton levels using several polarized PDFs
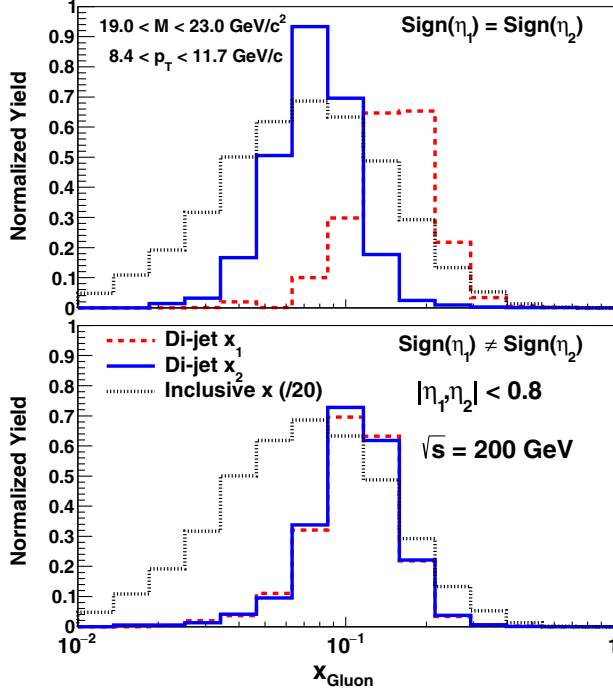
FIG. 3. Values of gluon x_1 and x_2 obtained from the PYTHIA detector level simulation for the same-sign (upper) and opposite-sign (lower) dijet topologies, compared to the gluon x distribution for inclusive jets scaled by an additional factor of 20 in each panel.
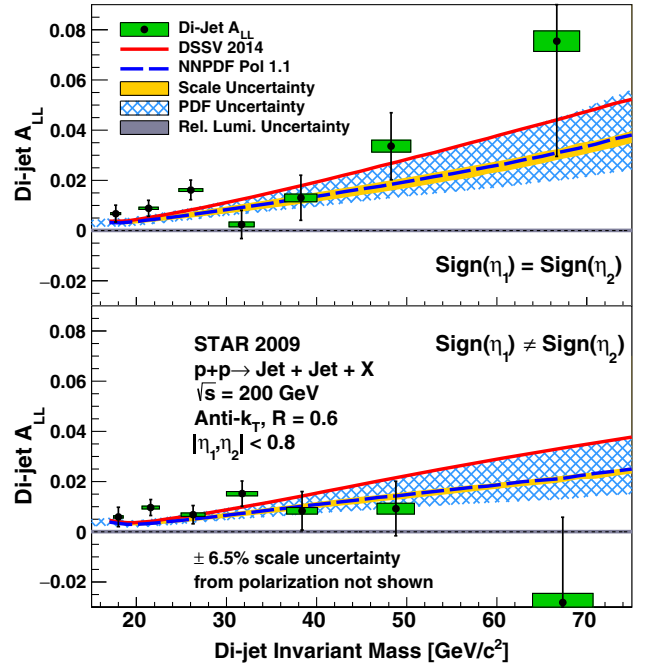

FIG. 4. Dijet A_{LL} vs parton-level invariant mass for the same-sign (top) and opposite-sign (bottom) topological configurations measured by the STAR experiment. The uncertainty symbols and theoretical curves are explained in the text.

which predict asymmetries that "bracket" the measured A_{LL} values. Although PYTHIA does not include parton polarization effects, asymmetries could be reproduced via a reweighting scheme in which each event was assigned a weight equal to the partonic asymmetry as determined by the hard-scattering kinematics and (un)polarized PDF sets. The trigger and reconstruction bias correction in each mass bin was determined by evaluating $\Delta A_{LL} \equiv A_{LL}^{\text{detector}} - A_{LL}^{\text{parton}}$ for each of the selected PDFs, then taking the average of the minimum and maximum values found. These corrections to A_{LL} varied from 0.0006 at low mass to 0.0048 at high mass. Half of the difference between the minimum and maximum ΔA_{LL} was taken as a systematic uncertainty on the correction.

Figure 4 presents the final dijet A_{LL} measurement for the same-sign (top) and opposite-sign (bottom) topological configurations as a function of dijet invariant mass, which has been corrected back to the parton level. The correction to parton level is achieved by shifting each point by the average difference between the detector and parton-level dijet masses for a given detector-level bin. The heights of the uncertainty boxes represent the systematic uncertainty on the A_{LL} values due to the trigger and reconstruction bias $(3–32 \times 10^{-4})$ and residual transverse polarization components in the beams $(3–26 \times 10^{-4})$. The relative luminosity uncertainty (5×10^{-4}) also results in an uncertainty in the

vertical dimension that is common to all points and is represented by the gray band on the horizontal axis. This uncertainty was evaluated by comparing relative luminosity values obtained using the STAR BBCs and ZDCs, as well as from quantitative inspection of a number of single- and double-spin asymmetries expected to yield null results. The widths of the boxes represent the systematic uncertainty associated with the corrected dijet mass values and, in addition to contributions from the uncertainty on the correction to the parton level, include uncertainties on calorimeter tower gains and efficiencies as well as TPC momentum resolution and tracking efficiencies. A further uncertainty was added in quadrature to account for the difference between the PYTHIA parton level and NLO pQCD dijet cross sections. This PYTHIA vs NLO pQCD uncertainty dominates in all but the lowest mass bin, rendering the dijet mass uncertainties highly correlated. The A_{LL} values and associated uncertainties can be found in Table I with more detail in the Supplemental Material [30].

Theoretical A_{LL} values were obtained from the dijet production code of de Florian *et al.* [7] using the DSSV2014 [17] and NNPDFpol1.1 [18] polarized PDF sets as input, normalized by the MRST2008 [33] and NNPDF2.3 [34] unpolarized sets, respectively. As was done for the unpolarized cross section, theoretical values were generated using the same jet-finding parameters as the data. Uncertainty bands representing the sensitivity to factorization and renormalization scale (solid) and polarized PDF uncertainty (hatched) were generated for the

TABLE I.   Dijet invariant mass and A_{LL} values with associated uncertainties for the same-sign (bins 1–7) and opposite-sign (bins 8–14) topologies.

Bin	Mass ± (Sys) [GeV/c^2]	A_{LL} ± (Stat) ± (Sys)
1	17.70 ± 0.56	0.0067 ± 0.0034 ± 0.0004
2	21.34 ± 1.07	0.0088 ± 0.0032 ± 0.0005
3	26.02 ± 1.33	0.0162 ± 0.0039 ± 0.0006
4	31.66 ± 1.39	0.0024 ± 0.0056 ± 0.0010
5	38.25 ± 1.79	0.0130 ± 0.0089 ± 0.0015
6	48.28 ± 2.17	0.0336 ± 0.0133 ± 0.0024
7	66.65 ± 2.56	0.0755 ± 0.0460 ± 0.0041
8	17.99 ± 0.54	0.0059 ± 0.0039 ± 0.0005
9	21.58 ± 0.96	0.0096 ± 0.0032 ± 0.0006
10	26.29 ± 1.32	0.0068 ± 0.0037 ± 0.0007
11	31.72 ± 1.72	0.0151 ± 0.0050 ± 0.0009
12	38.38 ± 1.70	0.0083 ± 0.0077 ± 0.0013
13	48.79 ± 2.07	0.0092 ± 0.0109 ± 0.0022
14	67.32 ± 3.35	−0.0282 ± 0.0340 ± 0.0036

NNPDF result. Overall, the data show good agreement with both the DSSV (same-sign $\chi^2/\mathrm{NDF} = 9.9/7$, opposite-sign $\chi^2/\mathrm{NDF} = 9.2/7$) and NNPDF (same-sign $\chi^2/\mathrm{NDF} = 12.0/7$, opposite-sign $\chi^2/\mathrm{NDF} = 8.8/7$) predictions. This is to be expected as both global analyses incorporated the STAR 2009 inclusive jet A_{LL} data, of which these results are a subset (the correlation matrix between the inclusive and dijet results can be found in the Supplemental Material [30]). However, for both topological configurations, the measured asymmetries tend to lie above the theoretical predictions at low invariant mass. This suggests the dijet data may prefer a somewhat higher gluon polarization at low x than the current global analyses.

The dijet asymmetry results presented here represent an important advance in the experimental investigation of the gluon polarization and will be the basis for future high statistics dijet measurements at STAR. Correlation

measurements capture a more complete picture of the hard-scattering kinematics and therefore, as shown in Fig. 3, offer better determination of the gluon momentum fraction than is possible with inclusive jet measurements. This improvement in x resolution will allow global analyses to constrain better the behavior of $\Delta g(x)$ as a function of x, thus reducing the uncertainty on extrapolations to poorly measured x regions and, ultimately, the integrated value of $\Delta g(x)$.

In summary, we report the first dijet unpolarized cross section and longitudinal double-spin asymmetry measurements from STAR in polarized pp collisions at $\sqrt{s} = 200$ GeV. The cross section result is consistent with NLO pQCD expectations and has the potential to constrain unpolarized PDFs. The A_{LL} results support the most recent DSSV and NNPDF NLO global analyses, which included 2009 RHIC data and found the first nonzero ΔG value for $x > 0.05$, and may indicate a slightly higher gluon polarization at lower x values.

[1] C. A. Aidala, S. D. Bass, D. Hasch, and G. K. Mallot, Rev. Mod. Phys. **85**, 655 (2013), and references therein.

[2] D. de Florian, R. Sassot, M. Stratmann, and W. Vogelsang, Phys. Rev. Lett. **101**, 072001 (2008); Phys. Rev. D **80**, 034030 (2009).

[3] J. Blümlein and H. Böttcher, Nucl. Phys. **B841**, 205 (2010).

[4] E. Leader, A. V. Sidorov, and D. B. Stamenov, Phys. Rev. D **82**, 114018 (2010).

[5] R. D. Ball, S. Forte, A. Guffanti, E. R. Nocera, G. Ridolfi, and J. Rojo (NNPDF Collaboration), Nucl. Phys. **B874**, 36 (2013).

[6] I. Alekseev *et al.*, Nucl. Instrum. Methods Phys. Res., Sect. A **499**, 392 (2003).

[7] D. de Florian, S. Frixione, A. Signer, and W. Vogelsang, Nucl. Phys. **B539**, 455 (1999).

[8] C. Adolph *et al.* (COMPASS Collaboration), Phys. Lett. B **718**, 922 (2013).

[9] A. Airapetian *et al.* (HERMES Collaboration), J. High Energy Phys. 08 (2010) 130.

[10] B. I. Abelev *et al.* (STAR Collaboration), Phys. Rev. Lett. **97**, 252001 (2006).

[11] B. I. Abelev *et al.* (STAR Collaboration), Phys. Rev. Lett. **100**, 232003 (2008).

[12] L. Adamczyk *et al.* (STAR Collaboration), Phys. Rev. D **86**, 032006 (2012).

[13] L. Adamczyk *et al.* (STAR Collaboration), Phys. Rev. Lett. **115**, 092002 (2015).

[14] A. Adare *et al.* (PHENIX Collaboration), Phys. Rev. Lett. **103**, 012003 (2009).

[15] A. Adare *et al.* (PHENIX Collaboration), Phys. Rev. D **79**, 012003 (2009).

[16] A. Adare *et al.* (PHENIX Collaboration), Phys. Rev. D **90**, 012007 (2014).

[17] D. de Florian, R. Sassot, M. Stratmann, and W. Vogelsang, Phys. Rev. Lett. **113**, 012001 (2014).

[18] E. R. Nocera, R. D. Ball, S. Forte, G. Ridolfi, and J. Rojo (NNPDF Collaboration), Nucl. Phys. **B887**, 276 (2014).

[19] O. Jinnouchi *et al.*, arXiv:nucl-ex/0412053.

[20] H. Okada *et al.*, Phys. Lett. B **638**, 450 (2006).

[21] B. Schmidke *et al.*, BNL C-A Dept. Report No. C-A/AP/490, http://public.bnl.gov/docs/cad/Pages/Home.aspx, 2013.

[22] K. H. Ackermann *et al.* (STAR Collaboration), Nucl. Instrum. Methods Phys. Res., Sect. A **499**, 624 (2003), and references therein.

[23] J. Kiryluk (for the STAR Collaboration), arXiv:hep-ex/0501072.

[24] M. Cacciari, G. P. Salam, and G. Soyez, J. High Energy Phys. 04 (2008) 063.

[25] M. Cacciari, G. P. Salam, and G. Soyez, Eur. Phys. J. C **72**, 1896 (2012).

[26] T. Sjostrand, S. Mrenna, and P. Z. Skands, J. High Energy Phys. 05 (2006) 026.

[27] P. Z. Skands, arXiv:0905.3418.

[28] GEANT 3.21, CERN Program Library.

[29] T. Adye, Report No. CERN-2011-006, pp. 313–318.

[30] See Supplemental Material at http://link.aps.org/supplemental/10.1103/PhysRevD.95.071103 for tables of values and associated systematic uncertainties.

[31] H. L. Lai, M. Guzzi, J. Huston, Z. Li, P. M. Nadolsky, J. Pumplin, and C.-P. Yuan, Phys. Rev. D **82**, 074024 (2010).

[32] H. Jung, D. Treleani, M. Strikman, and N. van Buuren, Report No. DESY-PROC-2016-01.

[33] A. D. Martin, W. J. Stirling, R. S. Thorne, and G. Watt, Eur. Phys. J. C **63**, 189 (2009).

[34] R. D. Ball *et al.* (NNPDF Collaboration), Nucl. Phys. **B867**, 244 (2013).